Disulfidptosis-related lncRNA prognosis model to predict survival therapeutic response prediction in lung adenocarcinoma

XIAOMING SUN[1*], JIA LI[2*], XUEDI GAO[3], YUBIN HUANG[4], ZHANYUE PANG[1], LIN LV[2], HAO LI[4], HAIBO LIU[1] and LIANGMING ZHU[2]

[1]Department of Thoracic Surgery, Jinan Central Hospital, Jinan, Shandong 250013, P.R. China; [2]Department of Thoracic Surgery, Jinan Central Hospital, Shandong University, Jinan, Shandong 250013, P.R. China; [3]Department of Ophthamology, Jinan Mingshui Eye Hospital, Jinan, Shandong 250200, P.R. China; [4]Department of Thoracic Surgery, Jinan Central Hospital, Shandong First Medical University, Jinan, Shandong 250013, P.R. China

Received November 21, 2023; Accepted April 19, 2024

DOI: 10.3892/ol.2024.14476

Abstract. Lung adenocarcinoma (LUAD) is the most common pathological type of lung cancer, and disulfidptosis is a newly discovered mechanism of programmed cell death. However, the effects of disulfidptosis-related lncRNAs (DR-lncRNAs) in LUAD have yet to be fully elucidated. The aim of the present study was to identify and validate a novel lncRNA-based prognostic marker that was associated with disulfidptosis. RNA-sequencing and associated clinical data were obtained from The Cancer Genome Atlas database. Univariate Cox regression and lasso algorithm analyses were used to identify DR-lncRNAs and to establish a prognostic model. Kaplan-Meier curves, receiver operating characteristic curves, principal component analysis, Cox regression, nomograms and calibration curves were used to assess the reliability of the prognostic model. Functional enrichment analysis, immune infiltration analysis, somatic mutation analysis, tumor microenvironment and drug predictions were applied to the risk model. Reverse transcription-quantitative PCR was subsequently performed to validate the mRNA expression levels of the lncRNAs in normal cells and tumor cells. These analyses enabled a DR-lncRNA prognosis signature to be constructed, consisting of nine lncRNAs; U91328.1, LINC00426, MIR1915HG, TMPO-AS1, TDRKH-AS1, AL157895.1, AL512363.1, AC010615.2 and GCC2-AS1. This risk model could serve as an independent prognostic tool for patients with LUAD. Numerous immune evaluation algorithms indicated that the low-risk group may exhibit a more robust and active immune response against the tumor. Moreover, the tumor immune dysfunction exclusion algorithm suggested that immunotherapy would be more effective in patients in the low-risk group. The drug-sensitivity results showed that patients in the high-risk group were more sensitive to treatment with crizotinib, erlotinib or savolitinib. Finally, the expression levels of AL157895.1 were found to be lower in A549. In summary, a novel DR-lncRNA signature was constructed, which provided a new index to predict the efficacy of therapeutic interventions and the prognosis of patients with LUAD.

Introduction

According to the 2020 Global Cancer Statistics report (1) , lung cancer is the leading cause of cancer-associated fatalities worldwide. Although lung cancer ranks second in terms of the incidence rate, its mortality rate remains the highest (2). Non-small cell lung cancer (NSCLC) comprises ~85% of all lung cancer cases, with almost 60% of patients experiencing local or distant metastasis. Among subtypes of NSCLC, lung adenocarcinoma (LUAD) is the most prevalent (3). Despite the availability of various treatment modalities, including surgery, chemotherapy, targeted therapy and immunotherapy, for the management of LUAD, the overall 5-year survival rate remains <20% (4). Therefore, gaining a comprehensive understanding of the underlying molecular mechanisms that drive the development of LUAD and the identification of novel therapeutic targets or biomarkers, are crucial for the effective improvement of patient prognosis.

In the field of cancer metabolic therapy, programmed cell death (PCD) fulfills a crucial role. A new form of PCD termed disulfidptosis has recently been reported, disulfidptosis is distinct from other forms of PCD such as necrosis, apoptosis, autophagy and ferroptosis (5). Disulfidptosis has been reported to be triggered by an increased uptake of cysteine, coupled with an insufficient availability of NADPH. The NADPH deficiency leads to the formation of disulfide bonds within actin cytoskeletal proteins, causing dysfunction and disruption of the actin network, ultimately resulting in cell death (5,6). Actin, a versatile cytoskeletal protein, is involved in numerous

Correspondence to: Dr Liangming Zhu, Department of Thoracic Surgery, Jinan Central Hospital, Shandong University, 105 Jie Fang Road, Jinan, Shandong 250013, P.R. China
E-mail: 201999000028@sdu.edu.cn

*Contributed equally

Key words: lung adenocarcinoma, disulfidptosis, lncRNA, disulfidptosis-related lncRNA, disulfidptosis related lncRNA signature

cellular processes, including transcription, translation, cell morphogenesis, cellular mechanics, intracellular transport and disulfide formation (7,8). Aberrations in the cytoskeleton have been reported to be associated with promoting and regulating PCD in both animal and plant systems (9,10); therefore, understanding the mechanisms underlying tumor-associated disulfidptosis is of importance in developing understanding of the induction of tumor cell death and the prevention of tumorigenesis.

Long non-coding RNAs (lncRNAs) are a class of RNA molecules exceeding 200 nucleotides in length (10), which, unlike coding RNAs, do not participate in protein translation. However, lncRNAs do exert a critical role in gene regulation. Increasing evidence has highlighted the importance of lncRNAs as key regulators, involved in various physiological and pathological processes through influencing of gene expression (11,12). In recent years, high-throughput sequencing technologies have enabled the identification of numerous non-coding genes that significantly impact both tumorigenesis and tumor progression. These lncRNAs have the ability to modulate not only the proliferation, differentiation, invasion and metastasis of cancer cells, but to also influence their metabolic reprogramming (13,14). The significant involvement of lncRNAs in tumorigenesis underscores their potential as promising targets for precision cancer treatment; however, the precise role of lncRNAs in relation to disulfidptosis in LUAD remains incompletely understood.

Therefore, the present study aimed to identify and validate a novel lncRNA-based prognostic marker associated with disulfidptosis, with the intent to enhance prognostic prediction for patients with LUAD. Furthermore, the disparities in cellular processes, signaling pathways and immune status between high-risk and low-risk groups was also performed. Ultimately, the goal was to construct a prognostic nomogram to assist in clinical decision-making and personalized management through the provision of an estimation of the survival probability for patients with LUAD.

Materials and methods

Clinical data collection for patients with LUAD. Clinical data for patients with LUAD, was obtained from The Cancer Genome Atlas (TCGA) database (https://gdc-portal.nci.nih.gov). RNA sequencing (RNA-seq) data, clinical patient information and somatic mutation data were obtained from the database. The dataset consisted of a total of 600 samples, including 59 normal samples and 541 tumor samples. To ensure the reliability of the prognostic analysis, samples that had missing or non-informative prognostic data and normal tissue were excluded from the present study. This resulted in a final cohort of 507 tumor samples that were used for further investigations. To assess the differences in characteristics among the selected sample group, a χ^2 test was performed (Table I). The selection of genes associated with disulfidptosis was based on a recently published relevant study (5).

Construction of a risk model associated with disulfidptosis. To identify lncRNAs that exhibited co-expression patterns with disulfidptosis-associated genes, Pearson's correlation analysis was performed. Screening criteria of $|R|\geq 0.4$ and $P<0.001$ were applied, resulting in the identification of 91 lncRNAs using the limma (version 3.54.2) R package (15). Subsequently, dimensionality reduction techniques were used to obtain disulfidptosis-related (DR)-lncRNAs with prognostic significance. This process involved two steps: First, univariate Cox regression analysis identified 17 DR-lncRNAs that showed significant associations with overall survival (OS) in patients with LUAD. Subsequently, to further reduce dimensionality and refine the selection of relevant DR-lncRNAs, the lasso algorithm was used to further screen these 17 DR-lncRNAs using glmnet (version 4.1.7) in R (16). Finally, nine DR-lncRNAs that exhibited significant associations with OS in patients with LUAD were identified. Using the glmnet (version 4.1.7) and survival (version 3.5.5) packages in R (16,17), a lasso logistic regression model was constructed, which was calculated as follows: Risk Score=$\sum_{i=1}^{n}$ ($LNCRNAExp_i$ $Coef_i$). Based on the median risk score, patients were then categorized into low and high-risk groups.

Risk model accuracy, independence evaluation and generation of the nomogram. To evaluate the predictive ability of the risk model for patients with LUAD, several analyses and visualizations were performed. Kaplan-Meier (K-M) curve analysis was performed using survival (version 3.5.5) and survminer (version 0.4.9) R packages to assess the survival outcomes of different risk groups based on the risk scores obtained from the model (18). K-M curves were used to determine whether the risk model could effectively stratify patients into distinct survival groups. The log rank test was used to calculate the P-value of K-M survival curves and the 'two stage' function in the TSHRC package (version 0.1.6), was used when survival curves crossed over (19). Receiver operating characteristic (ROC) curve analysis was performed using the survival (version 3.5.5), survminer (version 0.4.9) and time ROC (version 0.4) R packages to assess the predictive ability of the risk model over specific time intervals, such as 1, 3 and 5 years (18). Principal component analysis (PCA), using the limma (version 3.54.2) and scatterplot3d (version 0.3.44) R packages (20), was used for dimensionality reduction to visualize different subgroups of patients based on their risk scores. Univariate and multivariate Cox regression analysis performed using the survival (version 3.5.5) R package were used to assess the associations among the risk model, clinical factors and patient outcomes. Univariate Cox regression analysis was used to assess the individual impact of each variable, whereas multivariate Cox regression analysis was used to determine whether the risk model remained a reliable prognostic predictor after adjusting for other clinical variables.

Through combining the risk model and various clinical variables including sex, age, T, N and stage, a nomogram was generated to predict the survival probability of patients with LUAD using the rms (version 6.7.0), survival (version 3.5.5), survcomp (version 1.48.0) and regplot (version 1.1) R packages (21). A calibration curve was generated using the rms (version 6.7.0), survival (version 3.5.5), survcomp (version 1.48.0) and regplot (version 1.1) R packages to evaluate the accuracy of the column chart by comparing the predicted probabilities with the observed probabilities.

Table I. Clinical characteristics of 3 sets of data randomly generated using data from The Cancer Genome Atlas database.

Clinical features	Total set, n (%)	Train set, n (%)	Test set, n (%)	P-value
Age, years				0.8184
≤65	239 (47.14)	122 (48.03)	117 (46.25)	
>65	258 (50.89)	128 (50.39)	130 (51.38)	
Sex				0.451
Female	272 (53.65)	141 (55.51)	131 (51.78)	
Male	235 (46.35)	113 (44.49)	122 (48.22)	
Stage				0.668
I	272 (53.65)	131 (51.57)	141 (55.73)	
II	120 (23.67)	66 (25.98)	54 (21.34)	
III	81 (15.98)	41 (16.14)	40 (15.81)	
IV	26 (5.13)	13 (5.12)	13 (5.14)	
T stage				0.6613
1	169 (33.33)	87 (34.25)	82 (32.41)	
2	271 (53.45)	130 (51.18)	141 (55.73)	
3	45 (8.88)	23 (9.06)	22 (8.70)	
4	19 (3.75)	12 (4.72)	7 (2.77)	
N stage				0.177
0	327 (64.5)	162 (63.78)	165 (65.22)	
1	95 (18.74)	54 (21.26)	41 (16.21)	
2	71 (14)	31 (12.20)	40 (15.81)	
3	2 (0.39)	2 (0.79)	0 (0.00)	
M				>0.999
0	338 (66.67)	165 (64.96)	173 (68.38)	
1	25 (4.93)	12 (4.72)	13 (5.14)	

T, tumor; N, node; M, metastasis.

Functional enrichment analysis. To identify differentially expressed genes (DEGs) based on different risk groups by using the limma (version 3.54.2), criteria of |Log2FC|>1.0 and P<0.05 were applied (15). Once the DEGs had been identified, gene ontology (GO) analysis was performed to explore the biological functions associated with these genes using the clusterProfiler (version 4.6.2) and ggpubr (version 0.6.0) packages in R (22). GO analysis comprised three categories: Biological processes (BP), cellular components (CC) and molecular functions (MF). Additionally Kyoto Encyclopedia of Genes and Genomes (KEGG) analysis was performed using the clusterProfiler (version 4.6.2) R package to assess the signaling pathways associated with the DEGs. Finally, gene set enrichment analysis (GSEA) using the clusterProfiler (version 4.6.2) and limma (version 3.54.2) R packages was performed to investigate the differential signaling pathways involved in the low and high-risk groups.

The ESTIMATE algorithm was used to assess differences in the tumor microenvironment (TME) between the different risk groups using the limma (version 3.54.2) and estimate (version 1.10.13) R packages. The CIBERSORT algorithm using the limma (version 3.54.2) R package was employed to calculate the relative expression levels of 22 immune cells within different risk groups. Additionally, the single sample (ss)GSEA algorithm in the GSVA (version 1.46.0) and limma (version 3.54.2) R package was used to identify variations in immune cells and immune function across different risk populations (20). To evaluate the immune escape of tumor cells and their response to immune checkpoint inhibitors (ICIs) within different risk groups, the tumor immune dysfunction exclusion (TIDE) score was assessed using the limma (version 3.54.2) and ggpubr (version 0.6.0) R packages. Mutation frequencies and cancer maps for patients with LUAD were generated using the maftools (version 2.14.0) R package (23). Furthermore, tumor mutation burden (TMB) of patients in the different risk groups was analyzed using TCGA somatic mutation data. Based on the median TMB score, patients with LUAD were categorized into low and high-risk TMB groups. Differences in TMB and survival between the two risk sets were analyzed using the survival (version3.5.5) and survminer (version0.4.9) R packages. To predict drug responses in the different risk groups of patients with LUAD, the oncoPredict (version 0.2) and limma (version 3.54.2) R packages were employed (23). This package was used to calculate the half-maximal inhibitory concentration (IC50) values of commonly used anti-tumor drugs and to predict drug reactions in the various risk groups.

Cell culture and reverse transcription-quantitative (RT-q) PCR analysis. The human LUAD A549 cell line and the human normal lung epithelial BEAS-2B cell line were

purchased from Procell Life Science &Technology Co., Ltd. Cells were cultured in RPMI-1640 medium (Thermo Fisher Scientific, Inc.) supplemented with 10% fetal bovine serum (Gibco; Thermo Fisher Scientific, Inc). The cell cultures were maintained in a humidified environment at 37˚C with 5% CO_2. The cell density for RNA extraction was $1x10^6$. Total RNA was extracted using the TRIzol® reagent (Thermo, Fisher Scientific, Inc.), and cDNA was obtained by reverse transcription using a reverse transcriptase kit (Takara Biotechnology Co., Ltd.) . The cDNA was amplified using the SYBR™ Green (Hunan Accurate Bio-Medical Technology Co., Ltd.). RNA extraction, cDNA synthesis and qPCR were all performed according to the manufacturer's protocols. The reaction volume was 20 μl, including 10.0 μl SYBR ™ Green, 0.5 μl each primer, 2 μl cDNA and 7.0 μl nucleic acid-free water. The thermocycling conditions were as follows: Initial denaturation at 95˚C for 30 sec, followed by 40 cycles of 95˚C for 5 sec, 55˚C for 30 sec and 72˚C for 30 sec. β-actin was used as an internal control. The mRNA expression levels were quantified using the $2^{-\Delta\Delta Cq}$ method and normalized against expression levels of β-actin (24). The primer sequences used are presented in Table II.

Statistical analysis. All statistical analyses were performed using R software (version 4.2.2) and GraphPad Prism (version 8.0.2; Dotmatics). Differences between the two groups were assessed using Student's t-test. The log-rank test and two stage hazard rate comparison were used to assess differences between the K-M curves. Univariate and multivariate Cox regression analyses were performed to identify prognostic risk factors associated with LUAD. $P<0.05$ was considered to indicate a statistically significant difference.

Table II. lncRNA primer sequences

lncRNA	Sequence (3'-5')
Homo-β-actin	F: CCTTCCTGGGCATGGAGTC
	R: TGATCTTCATTGTGCTGGGTG
Homo-LINC00426	F: CACTCCCTACACGTTCTAACCA
	R: ATCCCCCATTTGCTGTGTC
Homo-TDRKH-AS1	F: CACCTCTAGGCCAATTACCG
	R: GGTGCCACTCATGATTCAACG
Homo-AC010615.2	F: CGGTGAACTGATGGTGCTGG
	R: GGCTCATGGTTGGGCTATCTTC
Homo-MIR1915HG	F: CCGCGCTCACGATTGCTTT
	R: GCAAGCAGCATATAGCCTCGG
Homo-TMPO-AS1	F: CAAAAGACCCCAGAGCCGA ACT
	R: TTGGGGCGTGGGCGAAG
Homo-GCC2-AS1	F: TTTCAGCACCCCAGGCTAGT
	R: TCACCGCCATCCTTGTTGTAG
Homo-AL157895.1	F: AGTTCTCTGAGGGATAAGGAA CAT
	R: TTCTAGGCATTCACAGGGTGC
Homo-U91328.1	F: ATGGGTCTCCGCTGATGCTT
	R: CTCAGACCTGTAGTCTTCCAC CAG
Homo-AL512363.1	F: CCTCTGTCTCACTTCAGCTGTT
	R: TGATTGGAAAACAAGACGC TGG

F, forward; R, reverse.

Results

Clinical data of patients with LUAD. The present study included a total of 507 patients with LUAD, who were divided into training and testing sets in a 1:1 ratio. The training set comprised 253 patients with LUAD and was used for constructing the prognostic model and identifying prognostic DR-lncRNAs. The remaining 254 patients with LUAD formed the testing set, which was used to evaluate the accuracy of the risk model developed from the training set. A comprehensive comparison of key clinical characteristics, including age, sex, grading and staging, as well as tumor (T), metastasis (M) and node (N) status, among the training set, the testing set and the total set of patients was performed (Table I). Statistical analysis revealed no statistically significant differences in these clinical characteristics among the three sets. These findings suggested that the training, testing and all sets were adequately matched in terms of important clinical variables, minimizing potential confounding effects when evaluating the accuracy of the prognostic model.

Construction of the DR-lncRNA risk model for LUAD. The experimental plan of the present study was summarized in a flow diagram (Fig. 1). Pearson's correlation analysis using the limma (version 3.54.2) R package (15) was performed on expression levels of ten disulfidptosis-associated genes using RNA-seq data from patients with LUAD, sourced from the TCGA database. This analysis identified 91 differentially expressed lncRNAs (Table SI). To visualize the connections between these ten disulfidptosis genes and the 91 lncRNAs, a co-expression network was constructed using a Sankey diagram (Fig. 2A). Subsequently, univariate Cox regression analysis was performed to identify DR-lncRNAs that were associated with OS, leading to the identification of 17 lncRNAs significantly correlated with survival (Fig. 2B). To further reduce dimensionality and refine the selection of relevant DR-lncRNAs, the lasso algorithm was used to further screen these 17 DR-lncRNAs. Finally, nine DR-lncRNAs were identified that exhibited significant associations with OS in patients with LUAD. (Fig. 2C and D). These DR-lncRNAs were identified as U91328.1, LINC00426, MIR1915HG, TMPO-AS1, TDRKH-AS1, AL157895.1, AL512363.1, AC010615.2 and GCC2-AS1. Using the expression levels of these nine DR-lncRNAs and the coefficients derived from the Cox regression model, a risk score was subsequently calculated. The risk score formula yielded the following calculation: Risk score=(-0.408862554222557 x U91328.1)+(-0.412743922052189 x LINC00426)+(0.23703345398073 x MIR1915HG)+(0.225351354331566 x TMPO-AS1)+(-0.329373779699515 x TDRKH-AS1)+(-0.552378924475953 x AL157895.1)+(0.377529261105432 x AL512363.1)+(-0.225534318729328 x AC010615.2)+(0.565660789000357 x GCC2-AS1). Additionally,

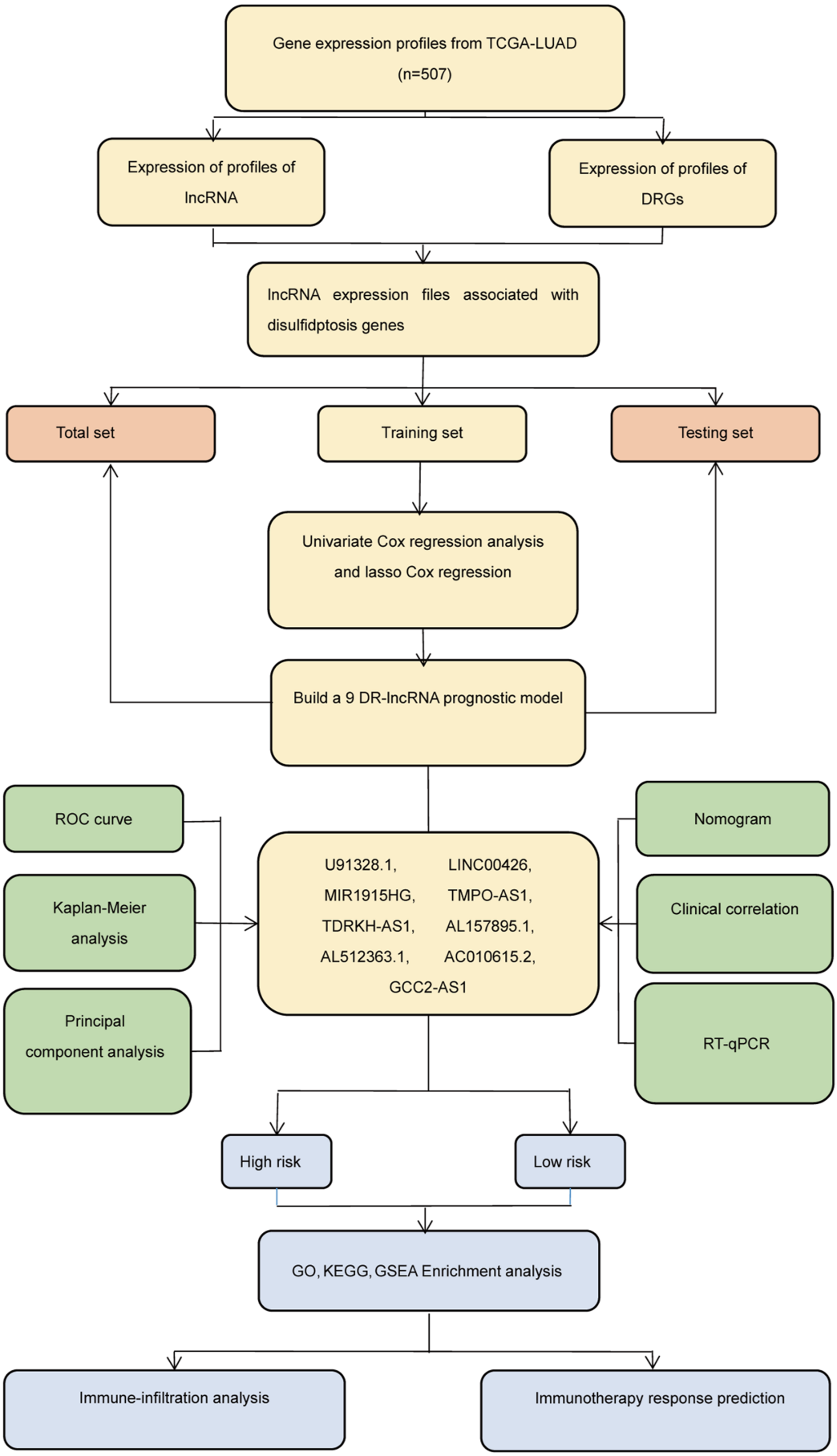

Figure 1. Schematic plan of the present study. TCGA, The Cancer Genome Atlas; LUAD, lung adenocarcinoma; lncRNA, long non-coding RNA; DRG, disulfidptosis-related gene; ROC, receiver operative characteristic; RT-qPCR, reverse transcription-quantitative PCR; GO, Gene ontology; KEGG, Kyoto Encyclopedia of Genes and Genomes; GSEA, gene set enrichment analysis.

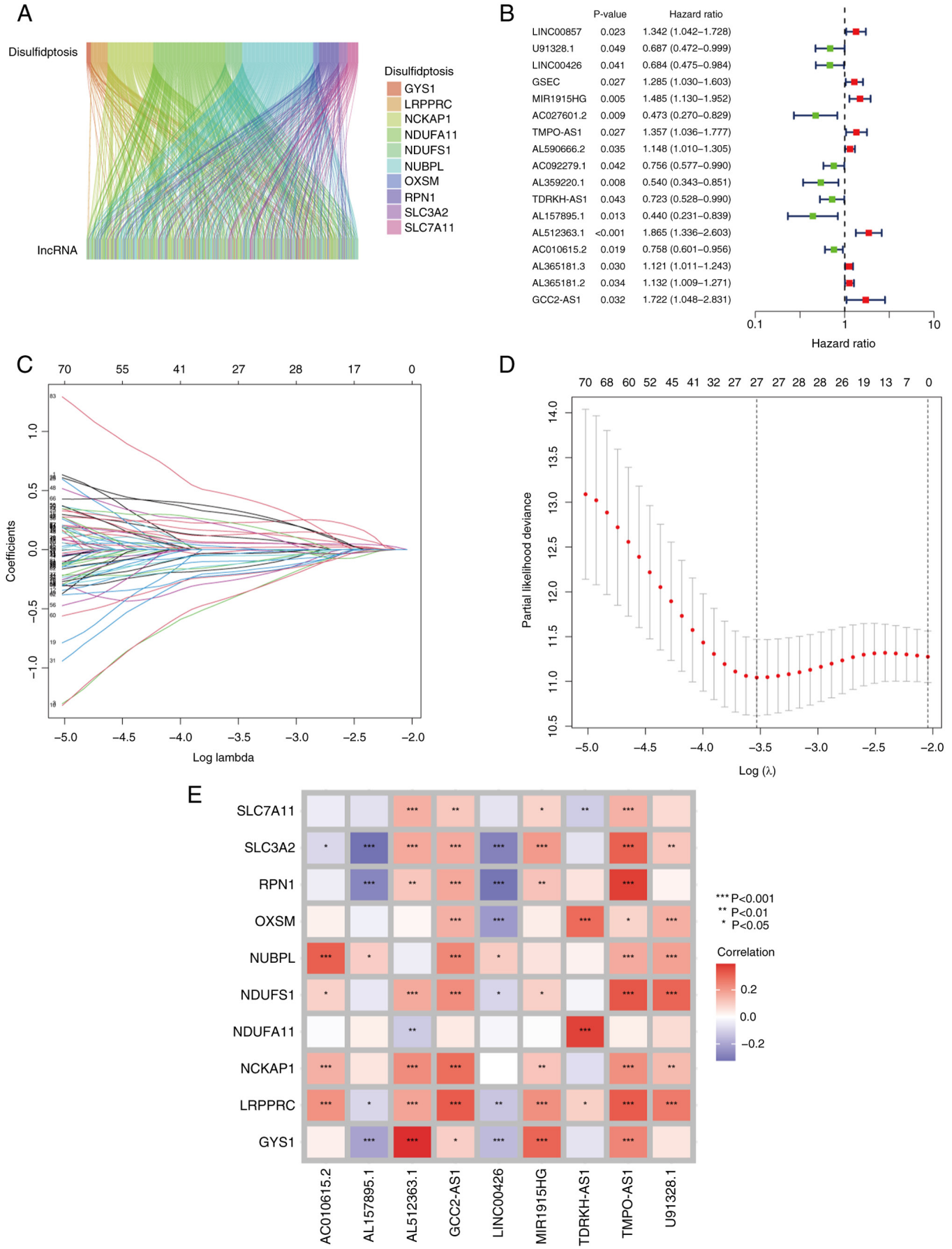

Figure 2. Construction of DR-lncRNA risk model. (A) Sankey diagram of the DR-lncRNAs associated with the ten disulfidptosis-associated genes (GYS1, LRPPRC, NCKAP1, NDUFA11, NDUFS1, NUBPL, OXSM, RPN1, SLC3A2 and SLC7A11). (B) Univariate Cox regression analysis indicated that the 17 lncRNAs were significantly associated with DR genes. (C and D) Lasso regression analysis identified nine DR-lncRNAs. (E) Correlation heatmap analysis of the ten DR genes, with nine independent prognosis lncRNAs. *P<0.05, **P<0.01 and ***P<0.001. DR-, disulfidptosis-related. DR, disulfidptosis-related.

correlation testing was performed to examine the association between the ten disulfidptosis genes and the nine DR-lncRNAs (Fig. 2E). This analysis provided valuable insights into the potential associations and interactions among these genes and lncRNAs in the context of disulfidptosis and LUAD.

Validation of the model of the disulfidptosis-related lncRNA signature (DRlncSig). The testing set and the total set of patient samples were used to assess the reliability of the established risk model. The risk curves and scatter plots of the test groups were generated to evaluate the performance of the risk model. The results demonstrated that, compared with the high-risk group, the low-risk group of patients with LUAD exhibited lower risk scores, longer survival times and an improved prognosis. A heatmap analysis was performed to investigate the potential role of the specific DRlncSig in LUAD. The heatmap indicated that MIR1915HG, TMPO-AS1, AL512363.1 and GCC2-AS1 may act as risk factors for LUAD (Fig. 3A). Furthermore, K-M curves were used to examine the differences in OS and progression-free survival (PFS) between the different risk groups. The results revealed that patients classified as low risk had significantly better OS and PFS values compared with those classified as high risk (Fig. 3C and D). These significant differences in the testing set were consistent with those observed in the total set of patients (Fig. 3B, E and F). Taken together, these findings suggested that the established risk model based on the identified DRlncSig was reliable and was capable of stratifying patients with LUAD into distinct risk groups with significantly different clinical outcomes in terms of OS and PFS.

Effectiveness evaluation of the DRlncSig. To evaluate the independent prognostic value of the DR-lncRNAs, both univariate and multivariate Cox regression analyses were performed. The results of the univariate Cox regression analysis showed that variables such as T, N, M, stage and risk score were significantly associated with OS in patients with LUAD (Fig. 4A). Subsequently, the multivariate Cox regression analysis demonstrated that the risk score could serve as an independent prognostic factor for predicting OS in patients with LUAD (Fig. 4B). Collectively, these findings suggested that the risk model constructed using the nine DR-lncRNAs had potential as an independent prognostic factor for patients with LUAD. Furthermore, ROC analysis (Fig. 4D) from the training set, testing set and total set, and C-index assessment from the total set (Fig. 4C) were performed to validate the prognostic capabilities of the lncRNA signature. The results obtained indicated that the risk score exhibited the highest area under the curve (AUC) value (AUC=0.706), and higher C-index, compared with other clinical risk indicators in the total set. In the training set, the AUC values at 1, 3 and 5 years were 0.689, 0.727 and 0.669, respectively. Similarly, in the testing set, the ROC curve showed AUC values of 0.663, 0.682 and 0.648 at 1, 3 and 5 years, respectively, providing strong evidence for the reliability of the model. In the total set, the AUC values at 1, 3 and 5 years were 0.673, 0.706 and 0.661 respectively (Fig. 4E). Additionally, a nomogram was generated, incorporating multiple clinical factors, including T, N, sex, age, stage and risk scores, to enhance the predictive ability of the prognosis of LUAD patients for 1-, 3- and 5-year survival (Fig. 4F). The calibration curve was used to assess accuracy of the nomogram, confirming its reliability (Fig. 4G).

K-M survival curve analysis of OS in high- and low-risk groups of TCGA database with different clinic-pathological characteristics. Further analysis was performed to examine the predictive ability of the constructed signature in subgroups with different clinical characteristics. The results illustrated that the risk model successfully differentiated between high- and low-risk groups, regardless of age, sex, TNM and the pathological stage (Fig. 5). These findings suggested that the established signature maintained its predictive ability across diverse subgroups with varying clinical characteristics. Therefore, the risk model based on the identified DR-lncRNAs was demonstrated to be robust and applicable for risk stratification in patients with LUAD, irrespective of demographic factors and disease stage.

Investigation of the grouping ability of the proposed model via PCA. PCA is a commonly used technique for dimensionality reduction, which transforms a large number of variables into a smaller set of principal components. These components retain most of the original dataset's information while reducing its dimensionality. In the present study, PCA was used to investigate whether the DRlncSig could effectively discriminate between the high- and low-risk patient groups. The results of the PCA analysis, presented in Fig. 6, clearly demonstrate a distinct separation between patients in the high- and low-risk groups on the basis of their DRlncSig profiles. Taken together, these findings suggested that the expression patterns of the identified DRlncSig had the potential to accurately differentiate between the high- and low-risk groups, suggesting that the DRlncSig may serve as a promising biomarker for either risk stratification or prognosis prediction in the studied disease context.

Functional enrichment analysis. To understand the underlying mechanisms contributing to the significant differences between the different risk groups, GO and KEGG enrichment analyses were performed, based on the nine identified DR-lncRNAs. The GO analysis revealed that the DEGs were significantly enriched in immune-related BP, including 'negative regulation of protein hydrolysis', 'humoral immune response', 'negative regulation of endopeptidase activity' and 'negative regulation of peptidase activity'. In terms of CC, these DEGs were notably enriched in the 'external side of plasma membrane' and the 'collagen-containing extracellular matrix'. Furthermore, in terms of MF, the DEGs were involved in 'receptor ligand activity' and 'signaling receptor activator activity' (Fig. 7A). Moreover, the KEGG enrichment analysis demonstrated that these DEGs were primarily enriched in pathways such as the 'PI3K-AKT signaling', 'amoebiasis' and 'focal adhesion' pathways (Fig. 7B). In addition, in the high-risk group, GSEA revealed significant enrichment of pathways associated with 'embryonic skeletal system morphogenesis', 'intermediate filament-based process' and the 'intermediate filament cytoskeleton' (Fig. 7C). However, the low-risk group exhibited significant enrichment of pathways associated with 'spliceosomal snRNP assembly' and the 'nucleosome' (Fig. 7D).

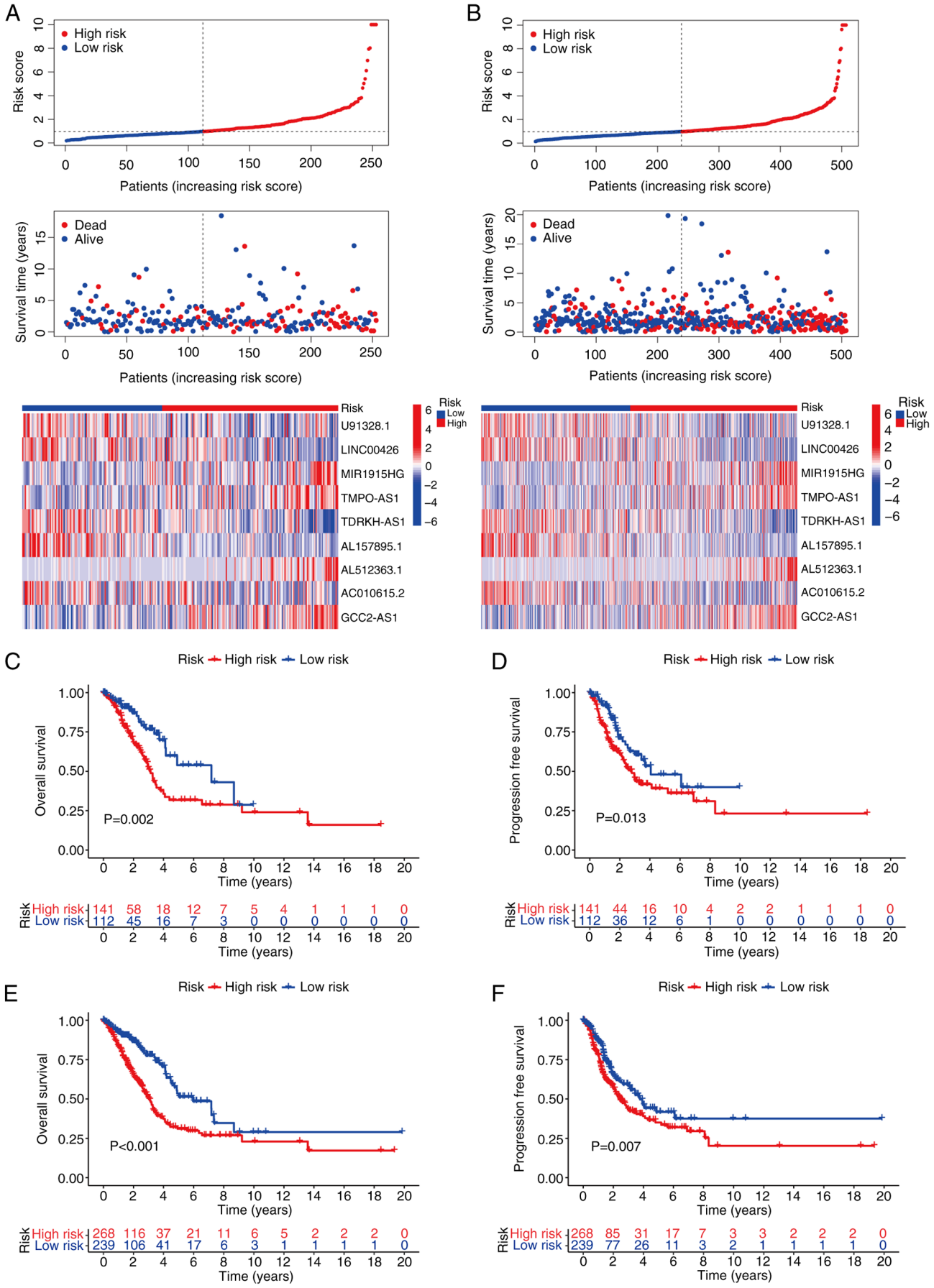

Figure 3. The model validation of the DRlncSig. (A) Distribution of risk scores, survival status and survival time patterns of patients in different risk groups in the testing set, along with the expression heatmap of the nine DR-lncRNAs. (B) Distribution of risk scores, survival status and survival time patterns of patients in the all set and the expression heatmap of the nine DR-lncRNAs. (C) OS and (D) PFS of patients in different risk groups in the testing set. (E) OS and (F) PFS of patients in different risk groups in the all set. DRlncSig, disulfidptosis-related lncRNA signature; OS, overall survival; PFS, progression-free survival.

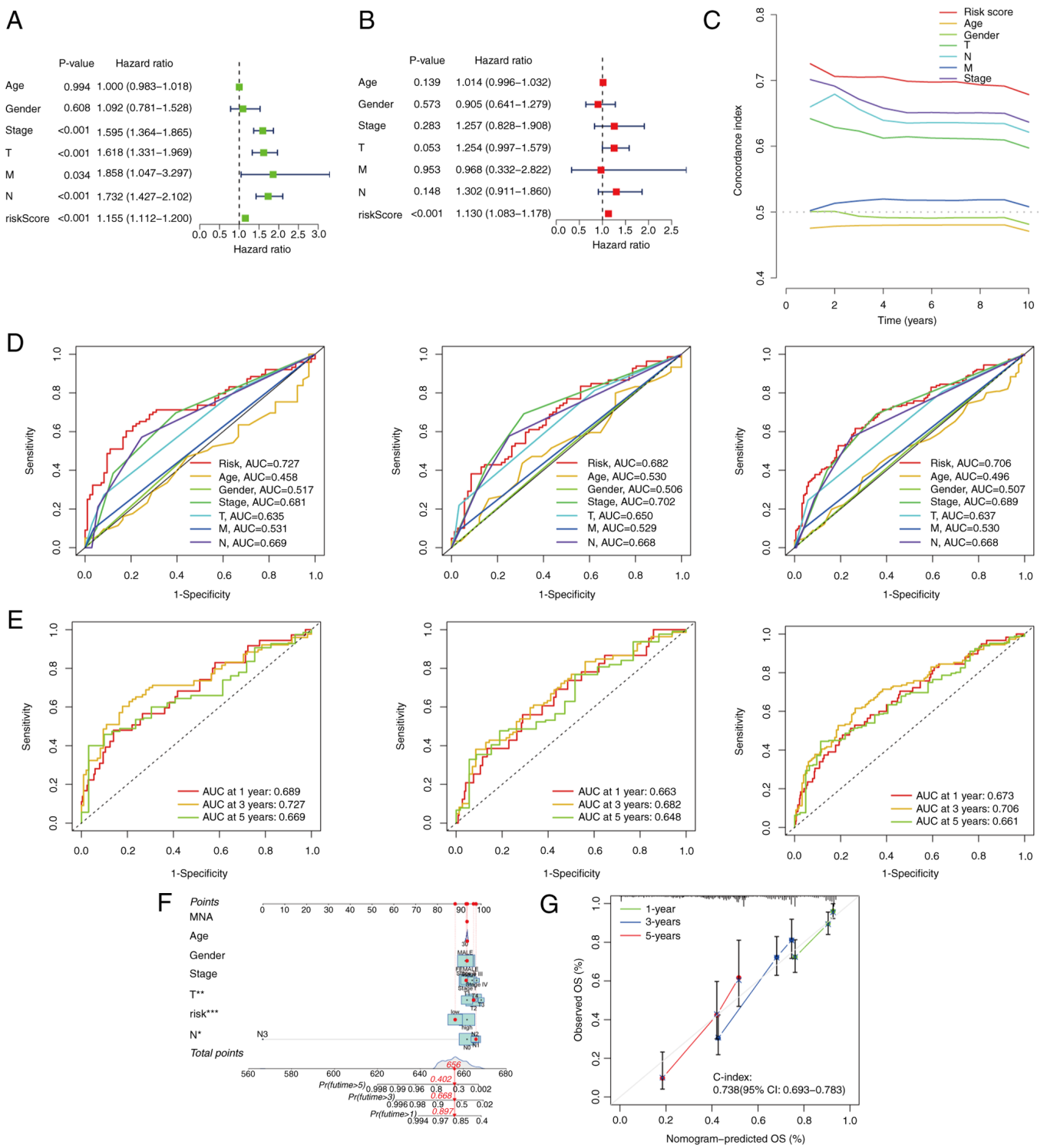

Figure 4. Effectiveness evaluation of the DRlncSig. Forest plots of (A) univariate and (B) multivariate Cox regression analysis. (C) C-index in the all set. (D) ROC curves of clinical risk indicators and risk scores in the training, testing and all sets. (E) ROC curves for 1-, 3- and 5-year OS in the risk model of the training, testing and all sets. (F) Nomogram and (G) calibration curves of the nomogram. DRlncSig, disulfidptosis-related lncRNA signature; OS, overall survival; ROC, receiver operating characteristic; T, tumor; N, node; M, metastasis.

Landscape analysis of immune infiltration and immunotherapy. The TME fulfills a crucial role in the progression and treatment of LUAD tumors (25,26). In the present study, the TME in the different risk groups was investigated using multiple immune evaluation algorithms. First, the ESTIMATE algorithm was used to assess TME scores. The immune score, ESTIMATE score and stromal score of patients with LUAD in the low-risk group were significantly higher compared with those in the high-risk group (Fig. 8A). These findings suggested that the TME characteristics differed between the two risk groups, potentially influencing both the prognosis and treatment response in patients with LUAD. Subsequently, the CIBERSORT algorithm was used to analyze the distribution of 22 immune cell types based on the risk model. The results

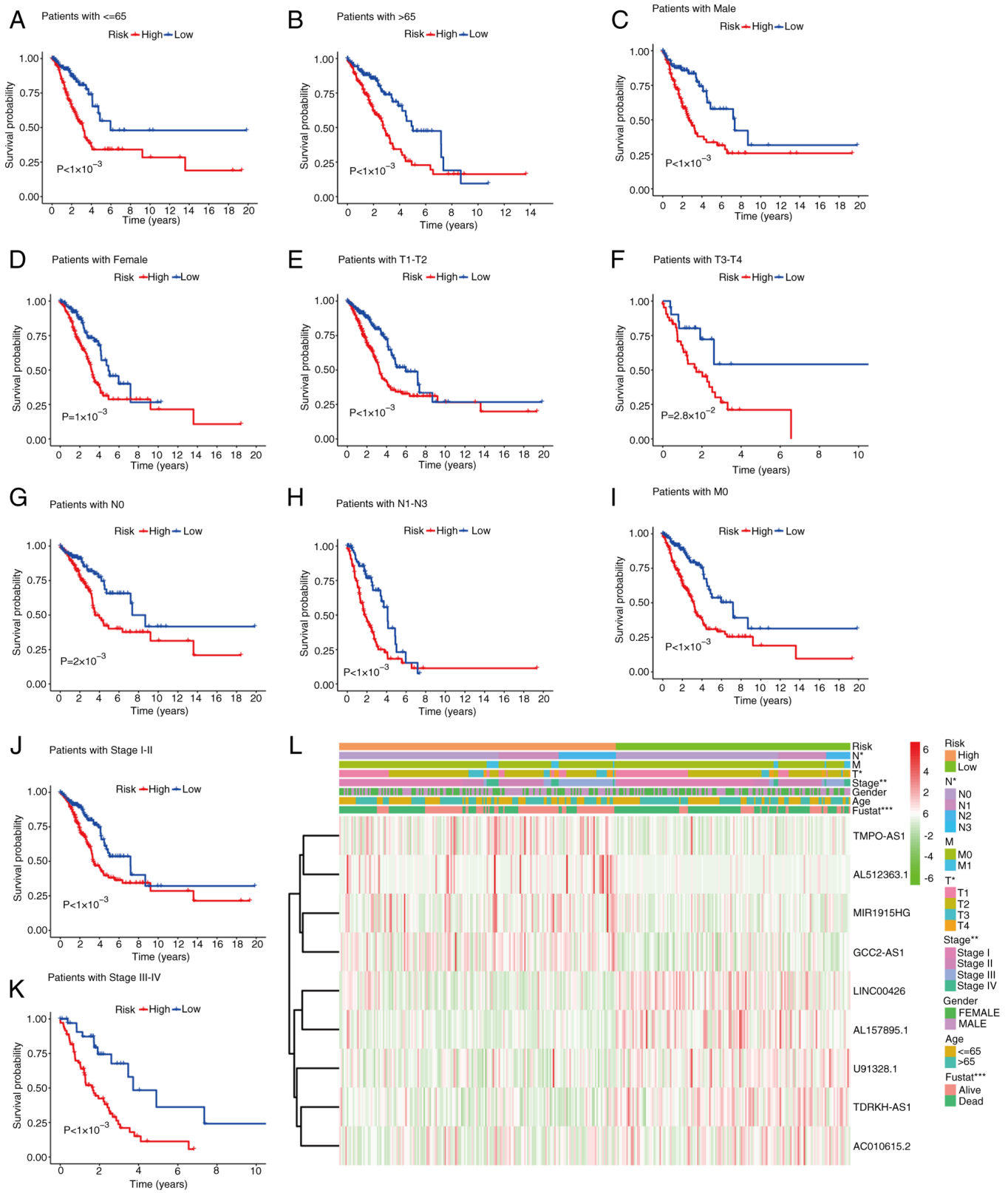

Figure 5. Kaplan-Meier survival curve analysis of the OS rate in the high- and low-risk groups of TCGA database with different clinical pathological characteristics: (A) age ≤65 years, (B) age >65 years, (C) males, (D) females, (E) T1-T2, (F) T3-T4, (G) N0, (H) N1-N3, (I) M0, (J) stage I-II and (K) stage III-IV. (L) Heatmap of the clinical pathological characteristics. *P<0.05, **P<0.01 and ***P<0.001. OS, overall survival; TCGA, The Cancer Genome Atlas; T, tumor; N, node; M, metastasis.

obtained indicated differences in the distribution of immune cells between the risk groups (Fig. 8B). Specifically, in the low-risk group, there was a lower proportion of M0 macrophages, activated mast cells and natural killer (NK) cells in the resting state compared with the high-risk group. However, resting memory CD4+ T cells, naive B cells, resting dendritic cells and resting mast cells accounted for a larger proportion in the low-risk group (Fig. 8C). Furthermore, the ssGSEA

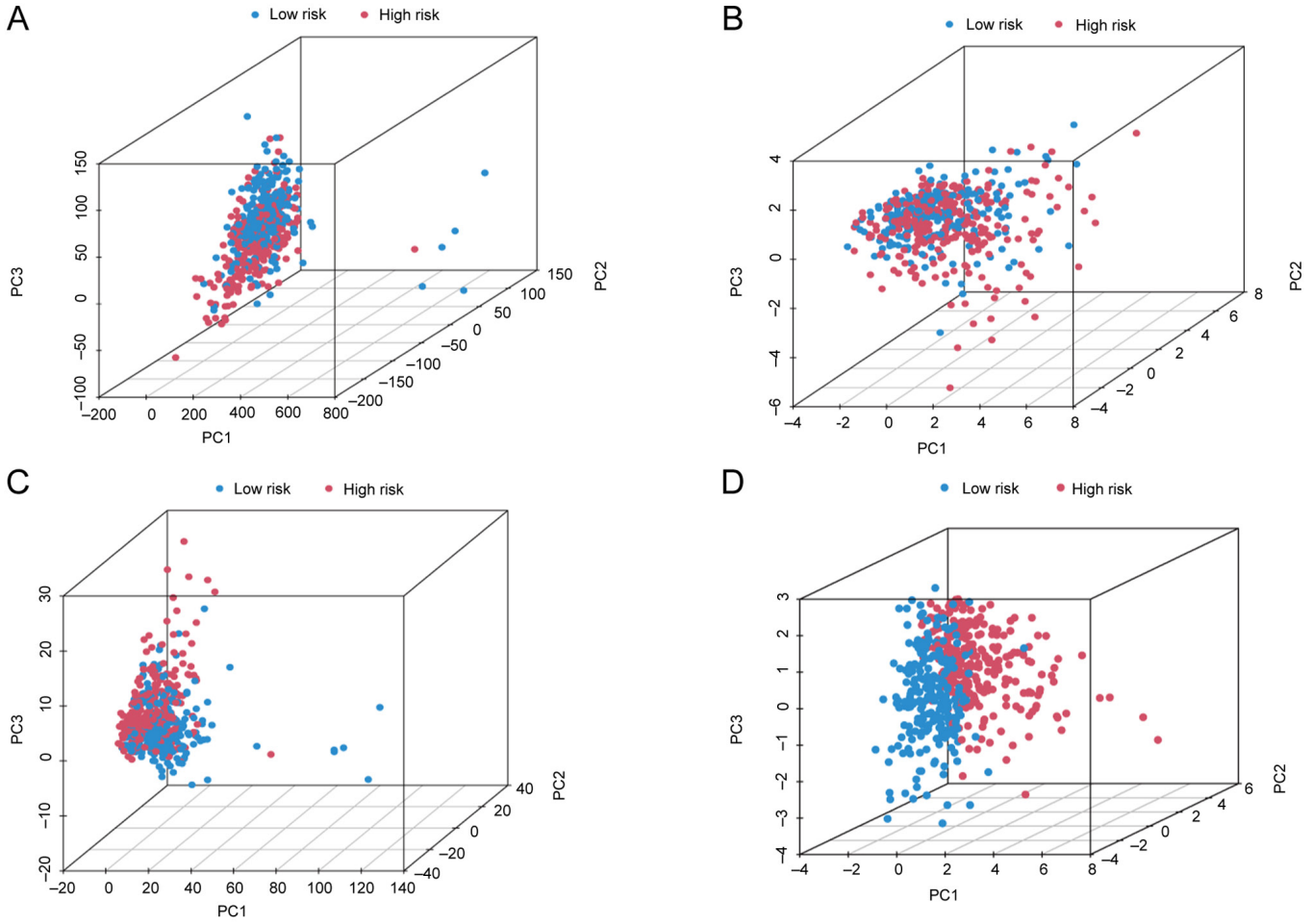

Figure 6. PCA in different groups. PCA for (A) gene expression, (B) the ten disulfidptosis-related genes, (C) DR-lncRNAs and (D) DRlncSig are shown. PCA, principal component analysis; DR, disulfidptosis-related; DRlncSig, disulfidptosis-related lncRNA signature.

algorithm was used to analyze immune cell infiltration and immune function in the different risk groups. The results demonstrated a significant increase in activated DCs), B cells, CD8+ T cells, DCs, mast cells, neutrophils, plasmacytoid DCs, T helper cells, T follicular helper, Th1 cells and tumor-infiltrating lymphocytes in the low-risk group. Regarding the immunological function, cytolytic activity, human leukocyte antigens, IDCS, T cell co-inhibition, T cell co-stimulation and type II IFN response were found to be significantly activated in the low-risk group (Fig. 8D). These findings suggested that the low-risk group may exhibit a more robust and active immune response against the tumor. Finally, the TIDE algorithm was used to estimate the relationship between the risk groups and immune therapy response. The results obtained suggested that tumors in the high-risk group were significantly more likely to experience immune escape, and to exhibit worse treatment effects (Fig. 8E).

Somatic mutation landscape analysis. A comparison of somatic mutations between the different risk groups was performed in the patients with LUAD. Among the 171 samples in the high-risk group, 158 samples (92.4%) had mutations, whereas in the low-risk group, 137 out of 154 samples (88.96%) had mutations. The top 15 genes driving these mutations were presented (Fig. 9A and B). Furthermore, the TMB was analyzed in the different risk groups; however, the difference was statistically significant (Fig. 9C). Subsequently, based on the median TMB score, patients with LUAD were divided into a low TMB and high TMB group. K-M analysis revealed that the high TMB group exhibited significantly improved OS rates compared with the low TMB group (Fig. 9D). To predict the prognosis of patients with LUAD and to determine which score had the greater predictive value, the TMB and risk scores were integrated. According to K-M analysis, patients with high TMB and low risk scores had the highest OS rate, whereas patients with low TMB and high-risk scores had the lowest OS (Fig. 9E).

Drug-sensitivity prediction. To improve the effectiveness and targeting of treatment for LUAD, the IC50 values of different anti-tumor drugs in the high- and low-risk groups were evaluated. The drug-sensitivity analysis revealed that samples in the high-risk group exhibited a significantly higher level of drug-sensitivity to crizotinib, erlotinib and savolitinib compared with samples in the low-risk group (Fig. 10A-C). However, high-risk group samples exhibited a significantly lower level of drug-sensitivity to axitinib, ribociclib and tozasertib compared with the low-risk group (Fig. 10D-F). These results suggested that patients in the low-risk group may have a more favorable response towards axitinib, ribociclib and

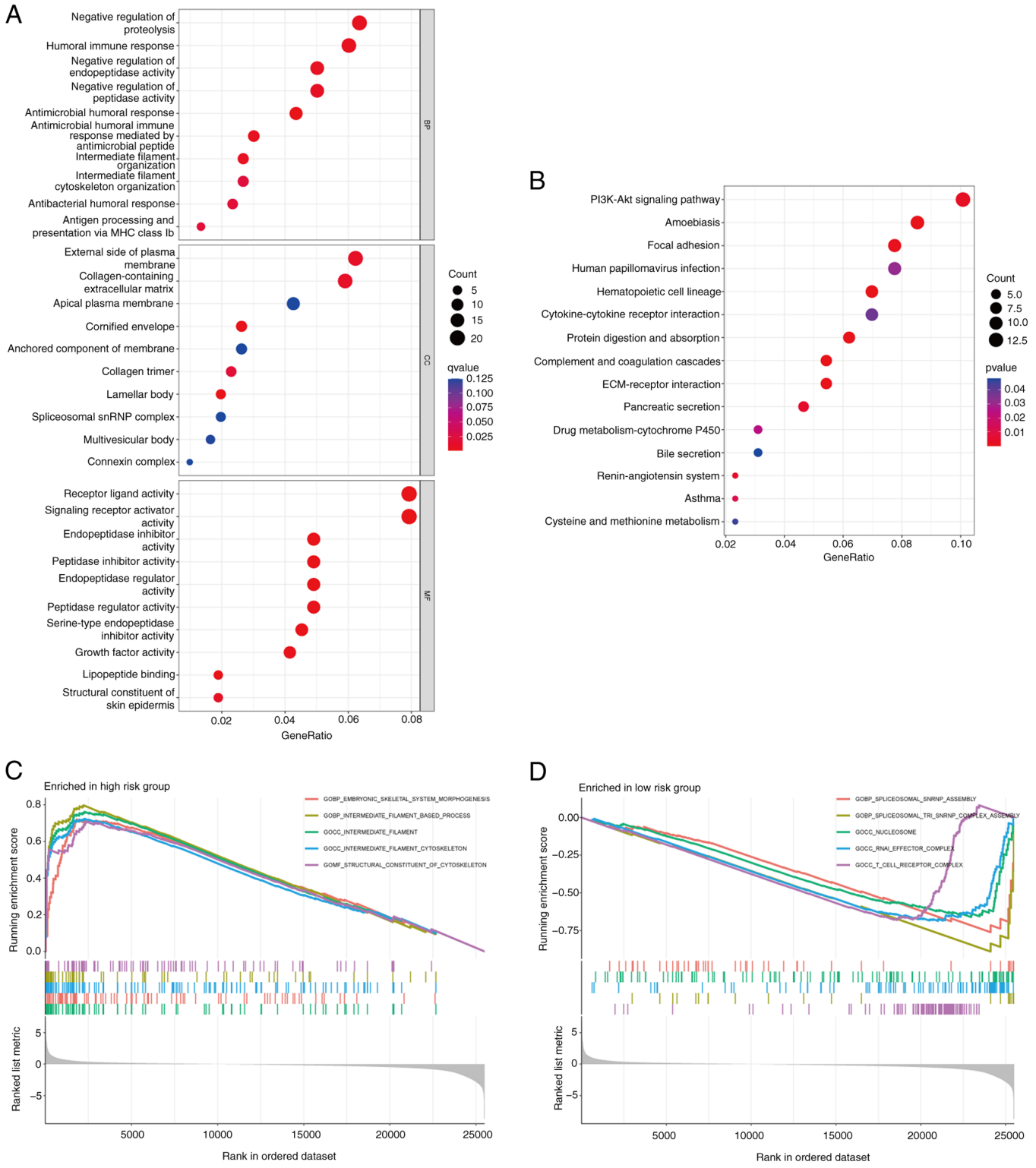

Figure 7. Functional enrichment analyses. (A) GO analysis, (B) KEGG analysis (15 pathways enriched in KEGG); (C) GSEA top 5 pathways enriched in the high-risk group; and (D) GSEA Top 5 pathways enriched in the low-risk group are presented. GO, Gene Ontology; KEGG, Kyoto Encyclopedia of Genes and Genomes; GSEA, gene set enrichment analysis.

tozasertib, whereas those in the high-risk group may respond better to treatment with crizotinib, erlotinib and savolitinib.

Cell-based in vitro experimental validation. To further validate the reliability of the risk model constructed using the DR-lncRNAs, RT-qPCR analysis was performed to assess the mRNA expression levels of DR-lncRNAs in LUAD. Subsequently, RT-qPCR analysis was performed on the A549 and BEAS-2B cells. The results obtained revealed significant differences in the expression levels of the eight tested DR-lncRNAs when compared between the normal and LUAD cell lines. Specifically, the mRNA expression

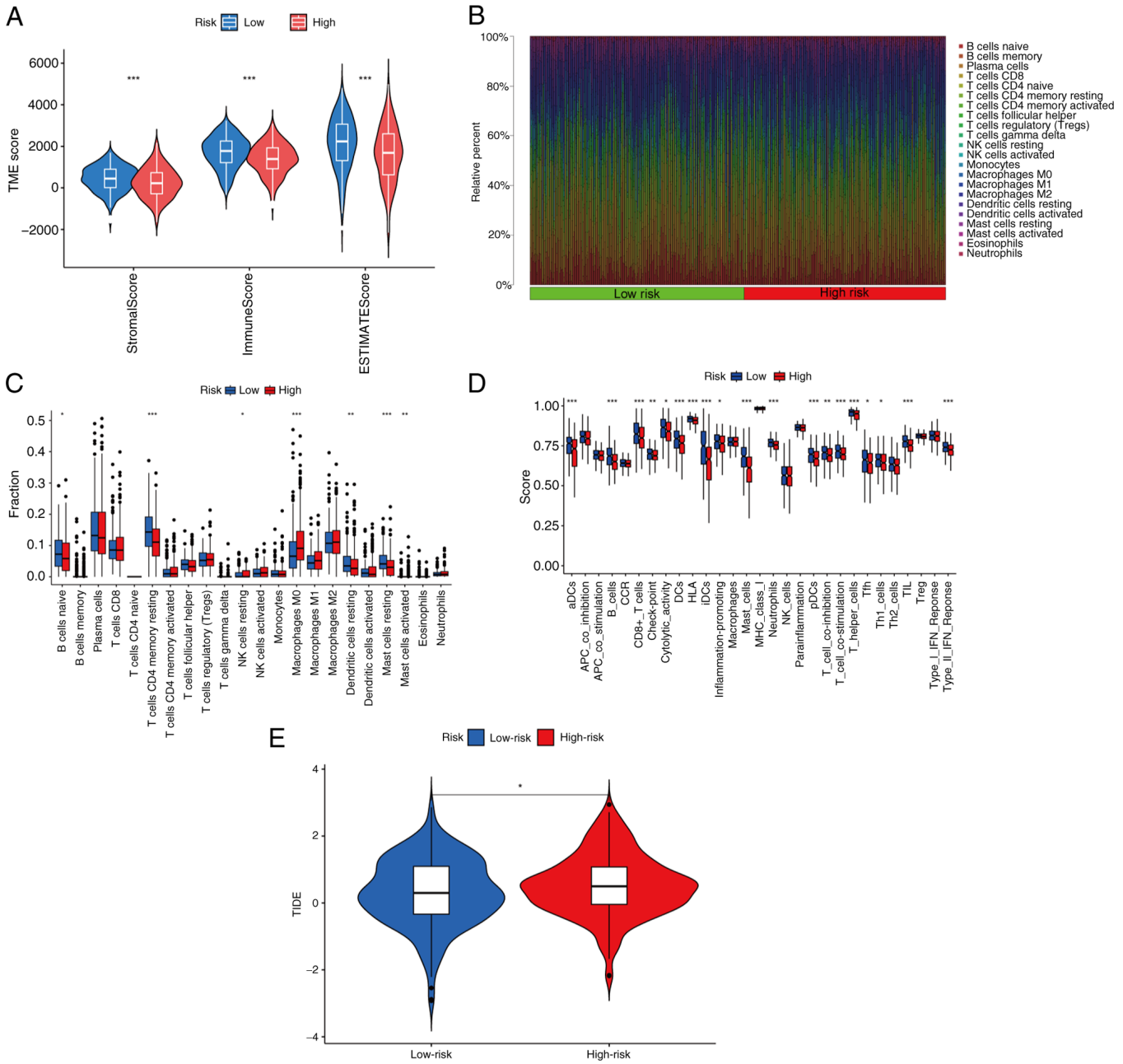

Figure 8. Immune infiltration landscape analysis and immunotherapy. (A) The ESTIMATE algorithm to assess the differences in the immune score, stromal score and estimate score between the two groups. (B and C) The CIBERSORT algorithm was used to evaluate the difference of 22 immune cells between the high- and low-risk groups. (D) The ssGSEA algorithm was used to analyze the differences in immune cells and immune function between the high- and low-risk groups. (E) TIDE score was calculated and compared between the high and low-risk groups. *P<0.05, **P<0.01 and ***P<0.001. ssGSEA, single-sample gene set enrichment analysis; TIDE, tumor immune dysfunction exclusion.

levels of U91328.1, AC010615.2, MIR1915HG, TMPO-AS1, LINC00426, TDRH-AS1, AL512363.1 and GCC2-AS1 were significantly higher in the A549 cells, compared with the BEAS-2B cells. Conversely, the mRNA expression level of AL157895.1 was significantly lower in the A549 cells (Fig. 11).

lncRNA GCC2-AS1 is overexpressed in LUAD. The validity of the model was demonstrated using lncRNA GCC2-AS1, which had the highest risk score coefficient. First, to compare the expression of GCC2-AS1 between the LUAD and normal tissues, its expression in tumor tissues and normal lung tissues was analyzed using data from TCGA database. GCC2-AS1 was demonstrated to be significantly upregulated in LUAD tissues (Fig. 12A). Additionally, in paired LUAD cancer samples and adjacent normal samples from TCGA, the expression level of GCC2-AS1 was significantly higher in LUAD samples compared with their matched adjacent normal samples (Fig. 12B). The aforementioned results were consistent with the aforementioned RT-qPCR results for GCC2-AS1 in the present study. An ROC analysis showed that GCC2-AS1 had a notable ability to discriminate between LUAD patients and healthy individuals, with an AUC of 0.761 (Fig. 12C), which suggested that GCC2-AS1 could be used to help identify people with LUAD. Subsequently, to examine the clinical relevance of GCC2-AS1

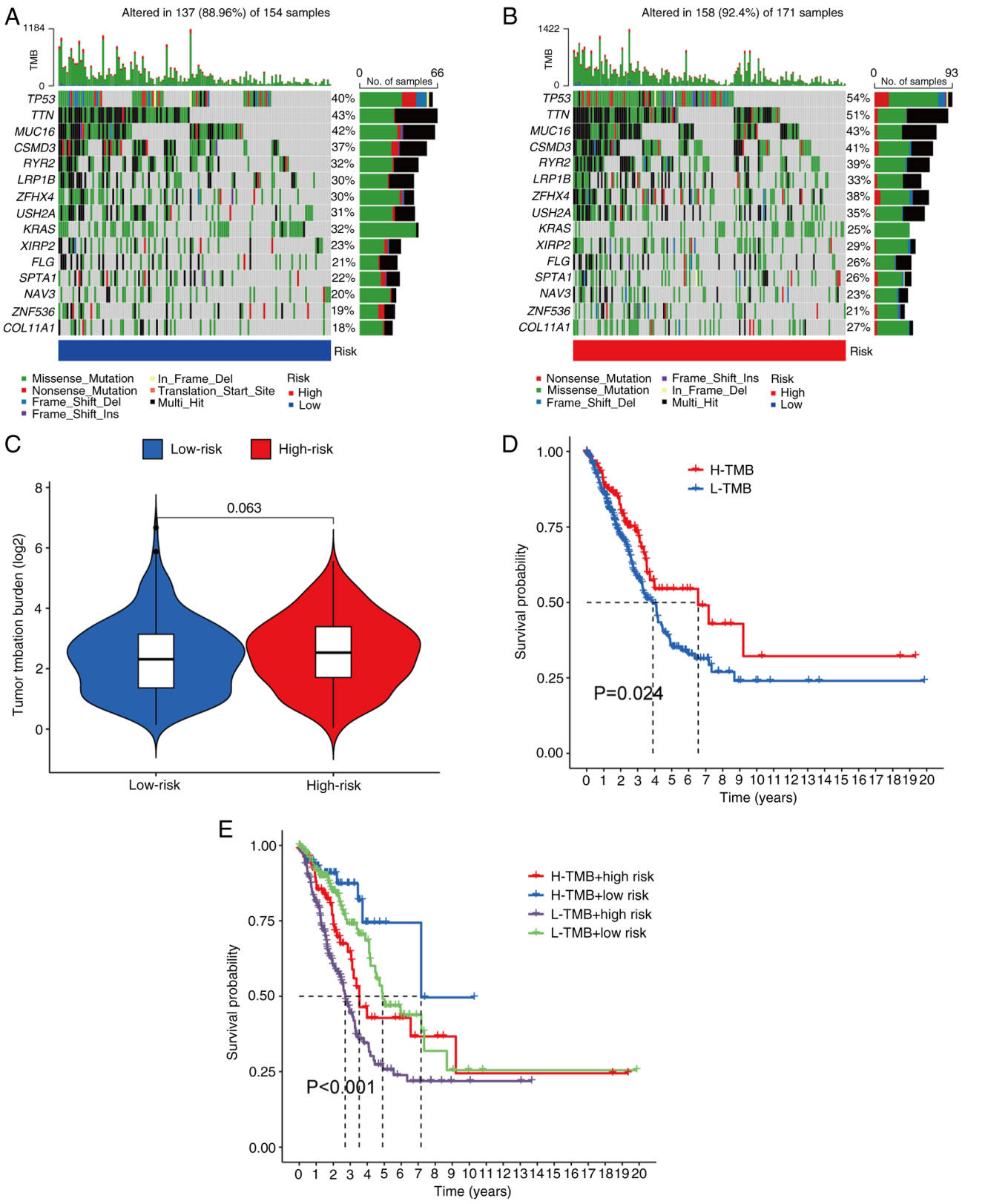

Figure 9. Analysis of the somatic mutation landscape. Mutation distribution of patients in the (A) low-risk group and (B) high-risk group. (C) Differences in TMB scores among different risk groups. (D) K-M analysis of OS of patients in the different TMB groups. (E) K-M analysis of OS among the four groups according to the TMB scores and risk scores. TMB, tumor mutation burden; K-M, Kaplan-Meier; OS, overall survival.

in LUAD, the patients with LUAD were divided into high and low-expression groups, based on the median expression level of GCC2-AS1. The correlations between GCC2-AS1 expression and clinical parameters, including stage, age and gender, were then evaluated. The results obtained showed significant statistical differences in the expression levels with respect to stage, gender and age (Fig. 12D). K-M analysis showed that patients with LUAD with a high-expression of GCC2-AS1 had

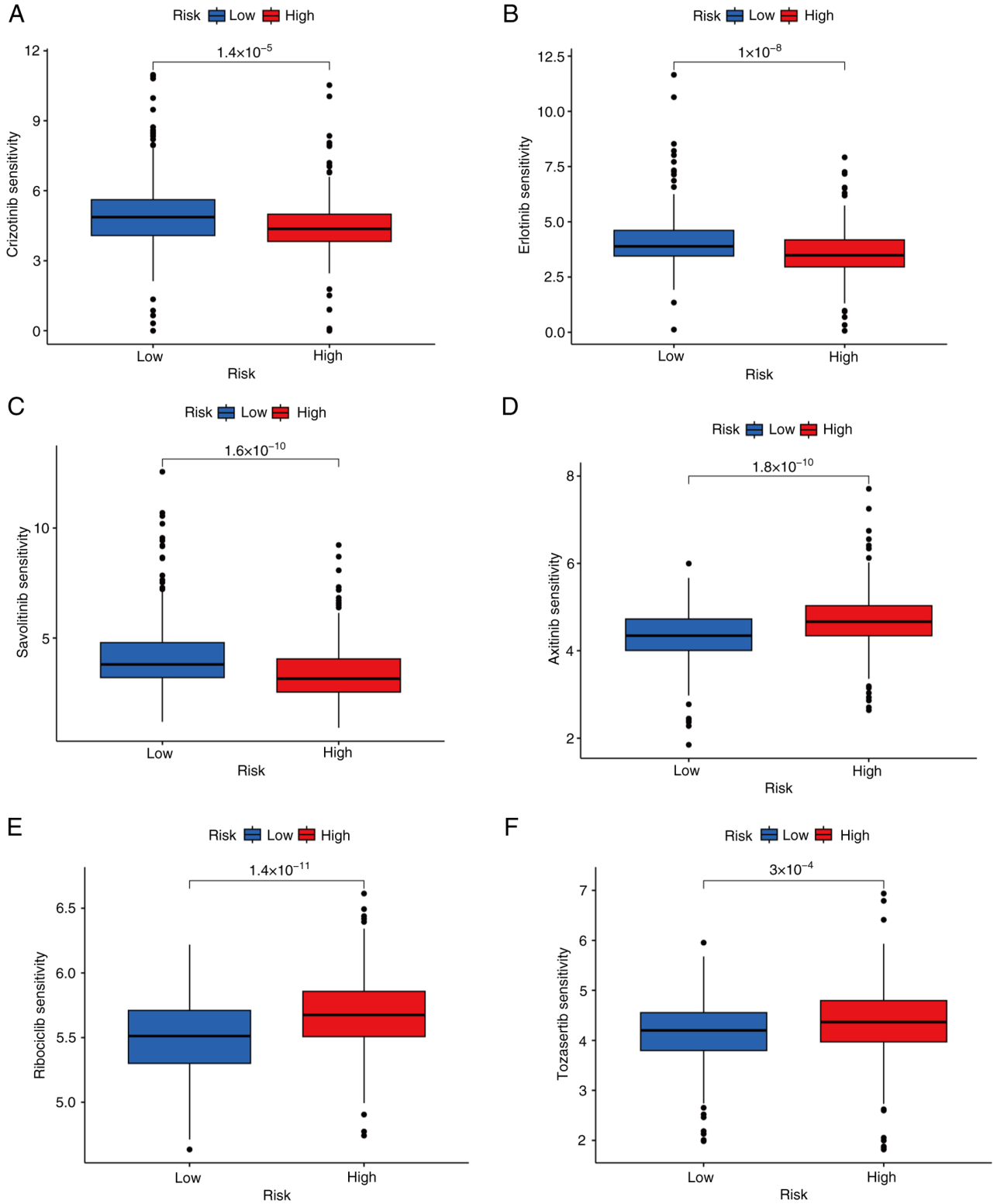

Figure 10. Analysis of therapeutic sensitivity. Sensitivities to (A) crizotinib, (B) erlotinib, (C) savolitinib, (D) axitinib, (E) ribociclib and (F) tozasertib.

significantly worse OS rates (Fig. 12E). Furthermore, ROC curve analysis revealed AUC values of 0.614, 0.601 and 0.590 at 1, 3 and 5 years, respectively, which indicated the reliability of GCC2-AS1 as a prognostic factor (Fig. 12F). To evaluate the independent prognostic value of GCC2-AS1, both univariate and multivariate Cox regression analyses were performed. The results of the univariate Cox regression analysis showed that variables such as T, N, stage and the expression of GCC2-AS1 were significantly associated with OS in patients with LUAD (Fig. 12G). Subsequently, multivariate Cox regression analysis indicated that GCC2-AS1 could serve as an independent prognostic factor for predicting OS in patients with LUAD (Fig. 12H). There have been few previous studies on the association between GCC2-AS1 and LUAD.

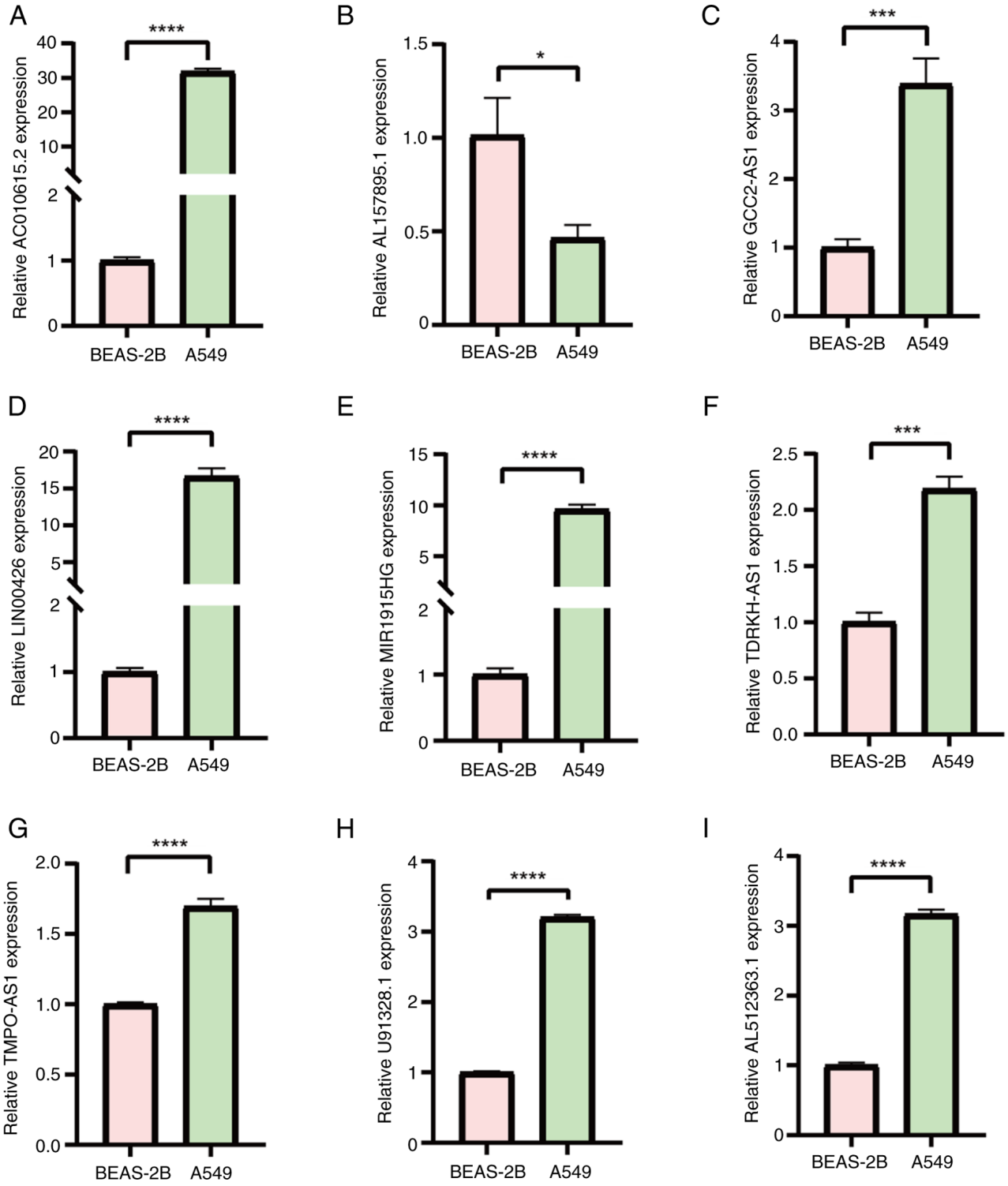

Figure 11. Expression levels of lncRNAs. Expression levels of (A) AC010615.2, (B) AL157895.1, (C) GCC2-AS1, (D) LIN00426, (E) MIR1915HG, (F) TDRKH-AS1, (G) TMPO-AS1, (H) U91328.1 and (I) AL512363.1 in BEAS-2B and A549 cells (*P<0.05, ***P<0.001 and ****P<0.0001).

Discussion

PCD is a fundamental process in multicellular organisms that regulates cell proliferation, maintains tissue homeostasis and eliminates harmful or unnecessary cells from the organism (27). Recently, a novel form of PCD termed disulfidptosis has been proposed (5). Disulfidptosis involves the accumulation of irreducible disulfides, leading to disulfide stress, and ultimately resulting in disulfide-driven apoptosis. Extensive research on lncRNAs has revealed their significant role in promoting or inhibiting various types of tumors, including LUAD, via the regulation of gene signals (28). LncRNAs are also potential biomarkers for diagnostic and prognostic purposes (29,30). However, the specific role of DR-lncRNAs in LUAD is very limited. For example, Zhang *et al* (31) identified 127 DRlncRNAs and established a prognostic model that consisted

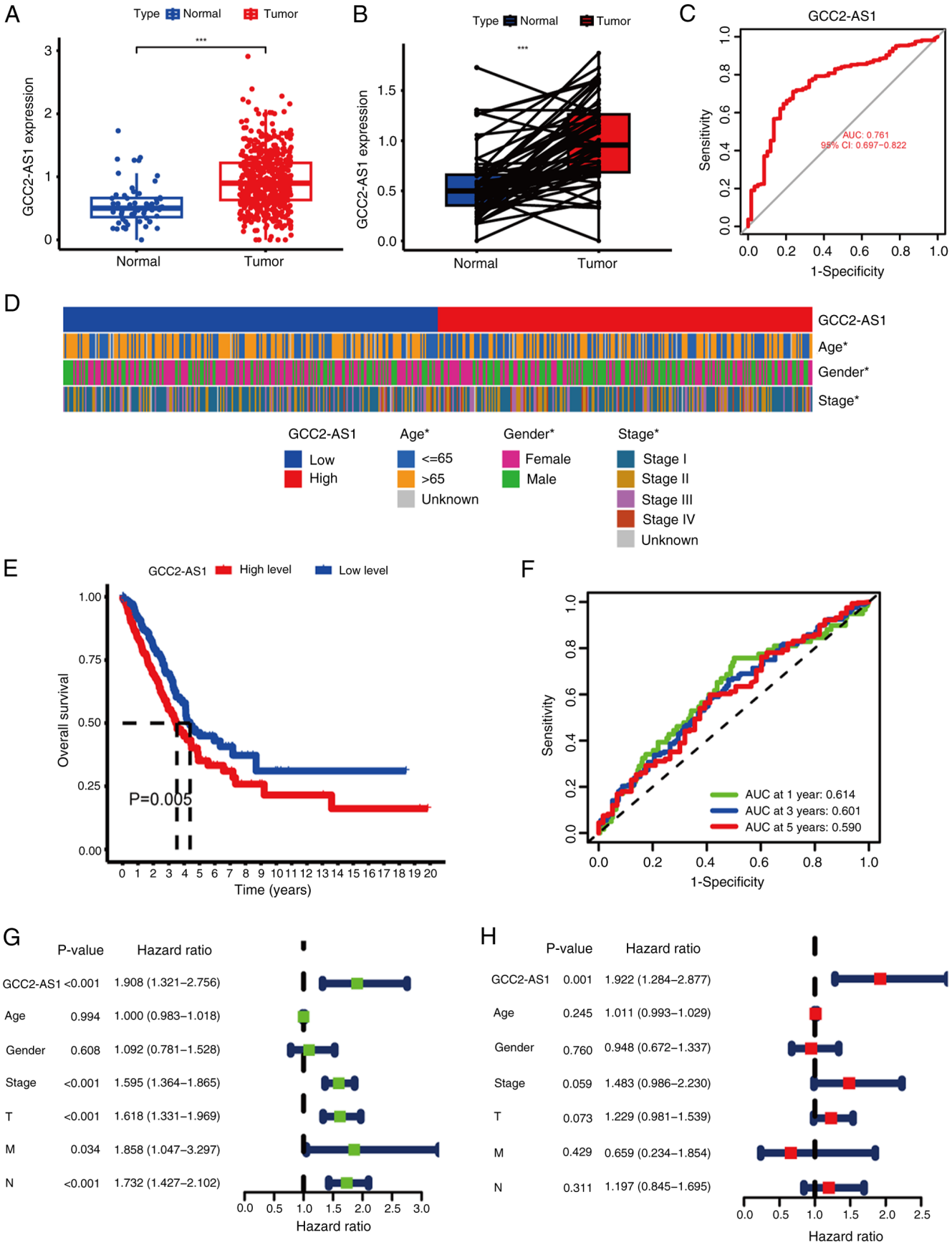

Figure 12. LncRNA GCC2-AS1 was overexpressed in LUAD. (A) Expression of the lncRNA GCC2-AS1 in LUAD based on TCGA-LUAD dataset. (B) Expression levels of the lncRNA GCC2-AS1 in paired adjacent normal tissues and paired samples. (C) ROC analysis of GCC2-AS1 expression indicates its high ability to discriminate tumor from non-tumor samples. (D) Heatmap of clinical pathological data. (E) The association between high and low expression of GCC2-AS1 and OS in the TCGA database. (F) ROC curves for 1-, 3- and 5-year OS in the expression levels of GCC2-AS1. Forest plots of (G) univariate and (H) multivariate Cox regression analysis. *P<0.05 and ***P<0.001. LUAD, lung adenocarcinoma; TCGA, The Cancer Genome Atlas; OS, overall survival; PFS, progression-free survival; ROC, receiver operating characteristic.

eight of them (KTN1-AS1, AL365181.3, MANCR, LINC01352, AC090559.1, AC093673.1, AP001094.3 and MHENCR) was verified. Song *et al* (32) developed a prognostic model based on a different set of five DRlncRNAs (AL365181.2, GSEC, AC093673.1, AC012615.1 and AL606834.1). The present study contributes to the growing body of research on the prognostic potential of DRlncRNAs in LUAD.

In the present study, univariate and lasso analyses were conducted, which lead to the identification of nine DR-lncRNAs associated with the prognosis of LUAD. Based on these findings, a prognostic model was constructed. Through the incorporation of clinical features and risk scores associated with prognosis, a nomogram was developed that could lead to an improvement in the prediction of OS in LUAD for 1, 3 and 5 years. To gain further insights into the differences between the high and low-risk groups, functional enrichment analysis was performed, and immune-associated data were analyzed. It was observed that patients with poor immunotherapy outcomes had higher risk scores. This suggested that the identified DR-lncRNAs may have a role in modulating the response to immunotherapy in LUAD. Integrating TMB with the risk score indicated potential for the provision of a more comprehensive prognostic assessment and in helping to identify patients with distinct OS outcomes. Furthermore, the present study also demonstrated that samples from the high-risk group of patients exhibited greater drug-sensitivity to crizotinib, erlotinib and savolitinib. This finding suggested that these targeted therapies may be of use in the treatment of LUAD, particularly in patients classified as high risk on the basis of the prognostic model. The research methodology of the present study is similar to those previously reported by Zhang *et al* (31) and Song *et al* (32), as lasso and Cox methods were used to construct a model of DRlncRNAs in LUAD. The risk model constructed using the DRlncRNA profiles identified in the present study, was similar to those previously reported by Zhang *et al* (31) and Song *et al* (32), and could also predict the prognosis of LUAD patients and their responses to immunotherapy and targeted therapy. Nevertheless, the lncRNA names identified in risk model of the present study differ from those reported in previous studies (31,32), which highlighted the importance of further identification of novel potential prognostic markers related to disulfidptosis in the present risk model. Variations in constructing risk models and identifying DRlncRNAs may arise from multiple factors, such as selecting different sets of disulfidptosis genes for the screening of DRlncRNAs. Specifically, as research related to disulfidptosis is in its early stages, the specific set of disulfidptosis genes has not yet been clearly defined. Guided by the principles of reliability and credibility, the 10 disulfidptosis genes selected in the present study were based on the initial study be Liu *et al* (5) which proposed disulfidptosis, representing the core genes initially identified for disulfidptosis, whereas the genes selected in the other two studies may have referenced additional literature (33,34), comprising 16 and 25 disulfidptosis genes, respectively. The risk model produced by the present study had a higher AUC value (AUC=0.727, compared to 0.673 (31) and 0.681 (32), which indicated that the present model may demonstrate greater clinical applicability, in terms of prognosis prediction. In summary, the present study adds to understanding of the prognostic significance of DRlncRNAs in LUAD, offering improved predictive models and highlighting potential therapeutic targets.

The signature used in the present study included nine lncRNAs, namely U91328.1, LINC00426, MIR1915HG, TMPO-AS1, TDRKH-AS1, AL157895.1, AL512363.1 and AC010615.2. Several of these lncRNAs have been previously reported in different cancer types. For example, U91328.1 has been reported to be associated with poor prognosis in colon cancer (35). TMPO-AS1 has previously been reported to be linked to ferroptosis and iron metabolism in LUAD (36). TDRKH-AS1 has been reported to promote the proliferation and invasion of colorectal cancer cells through the Wnt signaling pathway (37). LINC00426 has been reported to accelerate LUAD progression via the regulation of miR-455-5p (38). MIR1915HG has been reported to be associated with hypoxia in gastric adenocarcinoma (39). AL157895.1 has been reported to be associated with the occurrence and development of bladder cancer (40). However, to the best of our knowledge, no previously published studies have reported on roles for the other two lncRNAs, AL512363.1 and AC010615.2. The present study has shown that these nine lncRNAs may exert a role in the occurrence and development of LUAD and are closely associated with the underlying mechanism of disulfidptosis.

Changes which occur in the TME fulfill a crucial role in the progression of LUAD (25). The quantity and quality of tumor-infiltrating lymphocytes are key factors that forecast prognostic and therapeutic benefits in many types of cancer, such as lung adenocarcinoma, oral squamous cell carcinoma and epithelial ovarian cancer (41-44). The results of the present study suggested that the risk groups identified based on the prognostic model displayed distinct characteristics in terms of TME composition, immune cell distribution and immune function. Specifically, it was observed that the low-risk group exhibited a higher TME score. Furthermore, the present study revealed that the low-risk group exhibited increased immune cell infiltration and activation of immune function. Previous studies have found that an increased number of M0 macrophages is associated with poor prognosis in LUAD (45), while higher levels of CD8+ T lymphocyte and B lymphocyte infiltration are associated with better overall survival in LUAD (46), which is consistent with our research findings. This suggested that the immune system in the low-risk group is more responsive and active against tumor cells. By contrast, the high-risk group may have a more immunosuppressive TME, which could contribute to a reduced immune response and potential resistance to immune therapy. Considered together, these findings suggested that the immune profiles and TME characteristics differed between the high and low-risk groups. The low-risk group, with a more favorable immune profile, may have a better potential for positive treatment outcomes, including immunotherapy. These insights into the associations between risk groups, TME and immune function have provided information for understanding the immunological aspects of LUAD and may aid in the development of personalized treatment strategies.

ICIs have been reported to show promise as effective immunotherapies for numerous types of cancer. These inhibitors target specific molecules, such as programmed cell death protein 1 (PD-1)/programmed death-ligand 1 (PD-L1) and

cytotoxic T-lymphocyte associated protein 4, to enhance anti-tumor responses and to prevent tumor cells from evading immune surveillance (47,48). TMB has emerged as an important predictive marker for the response to ICIs (49-51). High TMB has been reported to be associated with a greater therapeutic efficacy of PD-1 or PD-L1 inhibitors (52). A study has reported the correlation between high TMB and improved treatment outcomes with ICIs (53). In the present study, the potential of the proposed markers to serve as reliable immune biomarkers for tumor treatment was assessed by analyzing the TMB and TIDE scores in the different risk groups. This analysis indicated the importance of somatic mutations and TMB in LUAD. Through the integration of TMB with the risk score derived from the prognostic model, the aim was to provide a more comprehensive prognostic assessment, and to identify patients with distinct OS outcomes. Overall, the findings of the present study indicated the importance of considering TMB and its integration with the risk score in evaluating immune responses and predicting treatment outcomes in LUAD. This information could be valuable for guiding personalized treatment decisions, and in of the improvement of patient outcomes in the context of immunotherapy.

As targeted therapy are conventional therapeutic strategies for intermediate and advanced LUAD (54), the sensitivity of anti-cancer drugs among different risk groups of patients with LUAD was also assessed. This analysis provided insights into individualized treatment strategies. Our results showed the IC50 values of targeted therapeutic agents such as crizotinib (55), erlotinib (56) and savolitinib (57) exhibited a notable decrease in patients with high risk scores, implying that these patients may display a more favorable treatment response to these drugs. With this approach, it will be possible to better match patients with the most appropriate anti-tumor drugs, leading to more effective and targeted therapies.

The present study did, however, have certain limitations. The disulfidptosis gene set selected was based on the study by Liu *et al* (5), and included GYS1, LRPPRC, NCKAP1, NDUFA11, NDUFS1, NUBPL, OXSM, RPN1, SLC3A2 and SLC7A11. It has subsequently been demonstrated that ACTB is also associated with disulfidptosis (58). In future studies, ACTB should be included in the gene set for disulfidptosis and in-depth research specifically targeting ACTB is required. Furthermore, the present data were derived from the TCGA database and lacked external dataset validation. Although the differential expression of these lncRNAs was validated in a LUAD cell line and a human normal cell line using RT-qPCR analysis, and bioinformatics analysis was performed to examine the expression of the lncRNA GCC2-AS1 and its relationship with lung adenocarcinoma, further *in vivo* and *in vitro* experiments are needed to confirm the impact of DR-lncRNAs on the occurrence and progression of LUAD.

In conclusion, in the present study a novel DRlncSig was constructed, which provided a novel index to predict the efficacy of therapeutic interventions and the prognosis of patients with LUAD, which could be used to guide personalized treatments.

Acknowledgements

Not applicable.

Funding

This study was financially supported by the Shandong Province Medical and Health Development Plan (grant no. 202304020860).

Availability of data and materials

The data generated in the present study may be requested from the corresponding author.

Authors' contributions

LZ, XS, JL and HLiu designed the study. JL performed the acquisition and analysis of bioinformatic data. XG, YH, ZP, LL and HLi performed cell culture and RT-qPCR analysis. XS wrote the manuscript. LZ edited the manuscript. All authors read and approved the final manuscript. XS and JL confirm the authenticity of all the raw data.

Ethics approval and consent to participate

Not applicable.

Patient consent for publication

Not applicable.

Competing interests

The authors declare that they have no competing interests.

Use of artificial intelligence tools

During the preparation of this work, AI tools were used to improve the readability and language of the manuscript or to generate images, and subsequently, the authors revised and edited the content produced by the AI tools as necessary, taking full responsibility for the ultimate content of the present manuscript.

References

1. Sung H, Ferlay J, Siegel RL, Laversanne M, Soerjomataram I, Jemal A and Bray F: Global Cancer Statistics 2020: GLOBOCAN estimates of incidence and mortality worldwide for 36 cancers in 185 countries. CA Cancer J Clin 71: 209-249, 2021.
2. Barta JA, Powell CA and Wisnivesky JP: Global epidemiology of lung cancer. Ann Glob Health 85: 8, 2019.
3. Zappa C and Mousa SA: Non-small cell lung cancer: Current treatment and future advances. Transl Lung Cancer Res 5: 288-300, 2016.
4. Spella M and Stathopoulos GT: Immune resistance in lung adenocarcinoma. Cancers (Basel) 13: 384, 2021.
5. Liu X, Nie L, Zhang Y, Yan Y, Wang C, Colic M, Olszewski K, Horbath A, Chen X, Lei G, *et al*: Actin cytoskeleton vulnerability to disulfide stress mediates disulfidptosis. Nat Cell Biol 25: 404-414, 2023.
6. Machesky LM: Deadly actin collapse by disulfidptosis. Nat Cell Biol 25: 375-376, 2023.
7. Ren W, Zhao W, Cao L and Huang J: Involvement of the actin machinery in programmed cell death. Front Cell Dev Biol 8: 634849, 2021.

8. Zhang Y and Chang SKC: Color and texture of surimi-like gels made of protein isolate extracted from catfish byproducts are improved by washing and adding soy whey. J Food Sci 87: 3057-3070, 2022.
9. Franklin-Tong VE and Gourlay CW: A role for actin in regulating apoptosis/programmed cell death: Evidence spanning yeast, plants and animals. Biochem J 413: 389-404, 2008.
10. Smertenko A and Franklin-Tong VE: Organisation and regulation of the cytoskeleton in plant programmed cell death. Cell Death Differ 18: 1263-1270, 2011.
11. Li Y, Jiang T, Zhou W, Li J, Li X, Wang Q, Jin X, Yin J, Chen L, Zhang Y, *et al*: Pan-cancer characterization of immune-related lncRNAs identifies potential oncogenic biomarkers. Nat Commun 11: 1000, 2020.
12. Li Y, Zhang J, Huo C, Ding N, Li J, Xiao J, Lin X, Cai B, Zhang Y and Xu J: Dynamic organization of lncRNA and circular RNA regulators collectively controlled cardiac differentiation in humans. EBioMedicine 24: 137-146, 2017.
13. Huarte M: The emerging role of lncRNAs in cancer. Nat Med 21: 1253-1261, 2015.
14. Luo J, Langer LF and Liu J: A novel role of LncRNA in regulating tumor metabolism and angiogenesis under hypoxia. Cancer Commun (Lond) 39: 2, 2019.
15. Xu M, Zhou H, Hu P, Pan Y, Wang S, Liu L and Liu X: Identification and validation of immune and oxidative stress-related diagnostic markers for diabetic nephropathy by WGCNA and machine learning. Front Immunol 14: 1084531, 2023.
16. Friedman J, Hastie T and Tibshirani R: Regularization paths for generalized linear models via coordinate descent. J Stat Softw 33: 1-22, 2010.
17. Yang M, Zheng H, Xu K, Yuan Q, Aihaiti Y, Cai Y and Xu P: A novel signature to guide osteosarcoma prognosis and immune microenvironment: Cuproptosis-related lncRNA. Front Immunol 13: 919231, 2022.
18. Chen Q, Sun T, Wang G, Zhang M, Zhu Y, Shi X and Ding Z: Cuproptosis-related LncRNA signature for predicting prognosis of hepatocellular carcinoma: A comprehensive analysis. Dis Markers 2022: 3265212, 2022.
19. Li H, Han D, Hou Y, Chen H and Chen Z: Statistical inference methods for two crossing survival curves: A comparison of methods. PLoS One 10: e0116774, 2015.
20. Wang F, Lin H, Su Q and Li C: Cuproptosis-related lncRNA predict prognosis and immune response of lung adenocarcinoma. World J Surg Oncol 20: 275, 2022.
21. Iasonos A, Schrag D, Raj GV and Panageas KS: How to build and interpret a nomogram for cancer prognosis. J Clin Oncol 26: 1364-1370, 2008.
22. Zhu N, Hou J, Si J, Yang N, Chen B, Wei X and Zhu L: SIRT1 and ZNF350 as novel biomarkers for osteoporosis: A bioinformatics analysis and experimental validation. Mol Biol Rep 51: 530, 2024.
23. Mayakonda A, Lin DC, Assenov Y, Plass C and Koeffler HP: Maftools: Efficient and comprehensive analysis of somatic variants in cancer. Genome Res 28: 1747-1756, 2018.
24. Livak KJ and Schmittgen TD: Analysis of relative gene expression data using real-time quantitative PCR and the 2(-Delta Delta C(T)) method. Methods 25: 402-408, 2001.
25. Wu J, Li L, Zhang H, Zhao Y, Zhang H, Wu S and Xu B: A risk model developed based on tumor microenvironment predicts overall survival and associates with tumor immunity of patients with lung adenocarcinoma. Oncogene 40: 4413-4424, 2021.
26. Yang L, He YT, Dong S, Wei XW, Chen ZH, Zhang B, Chen WD, Yang XR, Wang F, Shang XM, *et al*: Single-cell transcriptome analysis revealed a suppressive tumor immune microenvironment in EGFR mutant lung adenocarcinoma. J Immunother Cancer 10: e003534, 2022.
27. Christgen S, Tweedell RE and Kanneganti TD: Programming inflammatory cell death for therapy. Pharmacol Ther 232: 108010, 2022.
28. Tan C, Du H, Wang Y, Zhao J, Cheng X and Lan H: LncRNA GABPB1-IT1 inhibits the tumorigenesis of renal cancer via the miR-21/PTEN axis. J Biochem Mol Toxicol 37: e23288, 2023.
29. Cheng Z, Lu C, Wang H, Wang N, Cui S, Yu C, Wang C, Zuo Q, Wang S, Lv Y, *et al*: Long noncoding RNA LHFPL3-AS2 suppresses metastasis of non-small cell lung cancer by interacting with SFPQ to regulate TXNIP expression. Cancer Lett 531: 1-13, 2022.
30. Cui Y, Zhang C, Ma S and Guan F: TFAP2A-induced SLC2A1-AS1 promotes cancer cell proliferation. Biol Chem 402: 717-727, 2021.
31. Zhang HB, Pan JY and Zhu T: A disulfidptosis-related lncRNA prognostic model to predict survival and response to immunotherapy in lung adenocarcinoma. Front Pharmacol 14: 1254119, 2023.
32. Song Z, Cao X, Wang X, Li Y, Zhang W, Wang Y and Chen L: A disulfidptosis-related lncRNA signature for predicting prognosis and evaluating the tumor immune microenvironment of lung adenocarcinoma. Sci Rep 14: 4621, 2024.
33. Yang L, Liu J, Li S, Liu X, Zheng F, Xu S, Fu B and Xiong J: Based on disulfidptosis, revealing the prognostic and immunological characteristics of renal cell carcinoma with tumor thrombus of vena cava and identifying potential therapeutic target AJAP1. J Cancer Res Clin Oncol 149: 9787-9804, 2023.
34. Zhao S, Wang L, Ding W, Ye B, Cheng C, Shao J, Liu J and Zhou H: Crosstalk of disulfidptosis-related subtypes, establishment of a prognostic signature and immune infiltration characteristics in bladder cancer based on a machine learning survival framework. Front Endocrinol (Lausanne) 14: 1180404, 2023.
35. Zhou SZ, Pan YL, Deng QC, Yin CJ, Zhou DJ, Liu ML, Zhou J and Wu XJ: A prognostic signature for colon adenocarcinoma patients based on m6A-related lncRNAs. J Oncol 2023: 7797710, 2023.
36. Yao J, Chen X, Liu X, Li R, Zhou X and Qu Y: Characterization of a ferroptosis and iron-metabolism related lncRNA signature in lung adenocarcinoma. Cancer Cell Int 21: 340, 2021.
37. Jiao Y, Zhou J, Jin Y, Yang Y, Song M, Zhang L, Zhou J and Zhang J: Long non-coding RNA *TDRKH-AS1* promotes colorectal cancer cell proliferation and invasion through the β-Catenin activated *Wnt* signaling pathway. Front Oncol 10: 639, 2020.
38. Li H, Mu Q, Zhang G, Shen Z, Zhang Y, Bai J, Zhang L, Zhou D, Zheng Q, Shi L, *et al*: Linc00426 accelerates lung adenocarcinoma progression by regulating miR-455-5p as a molecular sponge. Cell Death Dis 11: 1051, 2020.
39. Fan Z, Wang Y and Niu R: Identification of the three subtypes and the prognostic characteristics of stomach adenocarcinoma: Analysis of the hypoxia-related long non-coding RNAs. Funct Integr Genomics 22: 919-936, 2022.
40. Zhang C, Bai X, Peng X, Shi W, Li Y, Chen G, Yu H, Feng Z and Deng Y: Starvation-induced long non-coding RNAs are significant for prognosis evaluation of bladder cancer. Aging (Albany NY) 14: 10067-10080, 2022.
41. Hwang C, Lee SJ, Lee JH, Kim KH, Suh DS, Kwon BS and Choi KU: Stromal tumor-infiltrating lymphocytes evaluated on H&E-stained slides are an independent prognostic factor in epithelial ovarian cancer and ovarian serous carcinoma. Oncol Lett 17: 4557-4565, 2019.
42. Paijens ST, Vledder A, de Bruyn M and Nijman HW: Tumor-infiltrating lymphocytes in the immunotherapy era. Cell Mol Immunol 18: 842-859, 2021.
43. Shaban M, Khurram SA, Fraz MM, Alsubaie N, Masood I, Mushtaq S, Hassan M, Loya A and Rajpoot NM: A novel digital score for abundance of tumour infiltrating lymphocytes predicts disease free survival in oral squamous cell carcinoma. Sci Rep 9: 13341, 2019.
44. Pan X, Lin H, Han C, Feng Z, Wang Y, Lin J, Qiu B, Yan L, Li B, Xu Z, *et al*: Computerized tumor-infiltrating lymphocytes density score predicts survival of patients with resectable lung adenocarcinoma. iScience 25: 105605, 2022.
45. Xue Q, Wang Y, Zheng Q, Chen L, Lin Y, Jin Y, Shen X and Li Y: Prognostic value of tumor immune microenvironment factors in patients with stage I lung adenocarcinoma. Am J Cancer Res 13: 950-963, 2023.
46. Liu X, Wu S, Yang Y, Zhao M, Zhu G and Hou Z: The prognostic landscape of tumor-infiltrating immune cell and immunomodulators in lung cancer. Biomed Pharmacother 95: 55-61, 2017.
47. Liu C, Zheng S, Wang Z, Wang S, Wang X, Yang L, Xu H, Cao Z, Feng X, Xue Q, *et al*: KRAS-G12D mutation drives immune suppression and the primary resistance of anti-PD-1/PD-L1 immunotherapy in non-small cell lung cancer. Cancer Commun (Lond) 42: 828-847, 2022.
48. Wen Y, Tang F, Tu C, Hornicek F, Duan Z and Min L: Immune checkpoints in osteosarcoma: Recent advances and therapeutic potential. Cancer Lett 547: 215887, 2022.
49. Jardim DL, Goodman A, de Melo Gagliato D and Kurzrock R: The challenges of tumor mutational burden as an immunotherapy biomarker. Cancer Cell 39: 154-173, 2021.
50. Liu L, Bai X, Wang J, Tang XR, Wu DH, Du SS, Du XJ, Zhang YW, Zhu HB, Fang Y, *et al*: Combination of TMB and CNA stratifies prognostic and predictive responses to immunotherapy across metastatic cancer. Clin Cancer Res 25: 7413-7423, 2019.

51. Samstein RM, Lee CH, Shoushtari AN, Hellmann MD, Shen R, Janjigian YY, Barron DA, Zehir A, Jordan EJ, Omuro A, *et al*: Tumor mutational load predicts survival after immunotherapy across multiple cancer types. Nat Genet 51: 202-206, 2019.
52. Ricciuti B, Wang X, Alessi JV, Rizvi H, Mahadevan NR, Li YY, Polio A, Lindsay J, Umeton R, Sinha R, *et al*: Association of high tumor mutation burden in non-small cell lung cancers with increased immune infiltration and improved clinical outcomes of PD-L1 blockade across PD-L1 expression levels. JAMA Oncol 8: 1160-1168, 2022.
53. Cao D, Xu H, Xu X, Guo T and Ge W: High tumor mutation burden predicts better efficacy of immunotherapy: A pooled analysis of 103078 cancer patients. Oncoimmunology 8: e1629258, 2019.
54. Imyanitov EN, Iyevleva AG and Levchenko EV: Molecular testing and targeted therapy for non-small cell lung cancer: Current status and perspectives. Crit Rev Oncol Hematol 157: 103194, 2021.
55. Shaw AT, Bauer TM, de Marinis F, Felip E, Goto Y, Liu G, Mazieres J, Kim DW, Mok T, Polli A, *et al*: First-line lorlatinib or crizotinib in advanced ALK-positive lung cancer. N Engl J Med 383: 2018-2029, 2020.
56. Abdelgalil AA, Al-Kahtani HM and Al-Jenoobi FI: Erlotinib. Profiles Drug Subst Excip Relat Methodol 45: 93-117, 2020.
57. Lee TS, Kim JY, Lee MH, Cho IR, Paik WH, Ryu JK, Kim YT and Lee SH: Savolitinib: A promising targeting agent for cancer. Cancers (Basel) 15: 4708, 2023.
58. Ni L, Yang H, Wu X, Zhou K and Wang S: The expression and prognostic value of disulfidptosis progress in lung adenocarcinoma. Aging (Albany NY) 15: 7741-7759, 2023.